Unsteady inflow conditions: A variationally based solution to the insurgence of pressure fluctuations

# Unsteady inflow conditions: a variationally based solution to the insurgence of pressure fluctuations

L. Patruno*, S. de Miranda

*DICAM, University of Bologna, Viale Risorgimento 2, 40136 Bologna, Italy*

**Abstract**

The application of unsteady inflow conditions represents an important aspect when scale resolving turbulence models are adopted in Computational Fluid Dynamics (CFD) analyses. In such context, with reference to Wind Engineering applications, the main concern is often represented by the generation of a synthetic velocity field representative of the turbulent fluctuations impinging on the studied body. Once such synthetic field has been generated, it is applied at the inflow patch. Unfortunately, such operation is not trivial: undesired pressure fluctuations are often generated due to the incompatibility between the applied inflow condition and the flow field found inside the computational domain. In this paper, a procedure able to guarantee a correct application of synthetically generated velocity fields to CFD simulations is described. The procedure, which relies on a variational background, is simple and can be readily implemented in existing codes. Numerical results confirm that, by adopting the proposed corrections, pressure fluctuations are strongly reduced, so confirming the soundness of the proposed approach. An OpenFoam implementation of the method is available for download at `https://site.unibo.it/cwe-lamc/en`.

*Keywords:* Synthetic turbulence, Inflow conditions, Pressure fluctuations, Large Eddy Simulation, VBIC

## 1. Introduction

Due to the recent wide spreading of scale resolving simulations in the field of Computational Fluid Dynamics (CFD), the generation and correct application of unsteady turbulent inflow conditions became a matter of remarkable importance. In fact, the presence of incoming turbulence has great effects on the majority of fluid flow problems and, as such, must be tackled in an appropriate way.

In particular, it is well known that the application of an unsteady velocity field as Boundary Condition (BC) of Dirichlet type at the inflow patch can cause strong pressure fluctuations [1, 2]. Such pressure fluctuations can be ascribed to three factors: the differential properties of the applied flow field (i.e. if the synthetic field fulfills in an exact or approximate way the Navier-Stokes equations or not), the presence of boundaries of the computational domain (other than the inflow patch) and effects induced by discretization [3, 4]. Such three aspects concur to establish if the applied inflow can be actually transmitted inside the CFD simulation. In particular, if the introduced velocity field does not respect the Navier-Stokes (NS) equations as well as the BCs, the velocity field must be modified in order to accommodate both such aspects. Such adaptation is mediated by the pressure field and leads to the insurgence of pressure fluctuations.

A thorough review of the literature regarding the generation of turbulent inflow conditions for CFD simulations is outside the scope of the present paper and the reader is invited to refer to [5, 6] which provide an extensive overview of the available techniques. Briefly, it can be said that available methodologies for the generation of inflow turbulence can be subdivided into two main categories: recycling methods and synthetic methods. The first ones generate the inflow conditions relying on appositely conceived CFD simulations while

*Corresponding author
*Email address:* `luca.patruno@unibo.it` (L. Patruno)

the second ones produce the fluctuating velocity field basing on analytical or semi-analytical formulations. In addition to such two categories, it is worth mentioning the volume forcing method in which turbulence is generated by adding source terms in the momentum equations in a zone upwind the location of interest (see for instance [7–9]). Despite the fact that the borders between such techniques are not always completely well defined, we notice that, in such last case, it might be better to speak about methods to promote the insurgence of turbulence rather than synthetic generation, as intended by the two other cited methodologies [10].

As regards recycling methods, the incoming turbulence is usually extracted from an auxiliary simulation or recycled within the simulation itself [11–15]. This implies that the unsteady flow field imposed at the inflow patch respects NS equations. Furthermore, if turbulence is recycled or the auxiliary simulation, as usual, has the same cross-wind domain size and BCs of the final simulation (between them only those which share at least one side with the inflow patch are relevant), the applied turbulence respects also the BCs. Such considerations are well known and explain the good performance of recycling methods, although this does not exclude that problems can arise due to numerical issues [16]. Nevertheless, the use of auxiliary simulations or recycling methods is unpractical and it would be strongly preferable to rely on synthetically generated inflow conditions.

Synthetically generated inflow conditions require to generate a time-varying synthetic turbulent field. At each time step, the trace of such field on the inflow patch is used in order to prescribe the velocity field. In general, such synthetic fields do not fulfill NS equations, nor they respect BCs. Such two aspects contribute to generate the aforementioned undesirable pressure fluctuations, together with the consequent modifications of the applied synthetic field.

A conspicuous amount of research has been recently devoted to generate synthetic turbulent fields useful for CFD computations. In particular, the primary objective has been to produce turbulent fluctuations characterized by prescribed statistical properties, usually in terms of time-spectra, Reynolds stresses and/or integral scales (see for example [17–21]). Such statistical properties are prescribed on the synthetic field but, due to the aforementioned modifications induced by the CFD simulation, there is no guarantee that they will be actually transmitted unaltered inside the CFD simulation.

In order to minimize such undesired modifications, numerous turbulence generation methods have been developed, aiming at prescribing to the synthetic field properties which ameliorate its compatibility with the NS equations. To this aim, synthetic turbulence generation methods which take into account the divergence-free condition and/or Taylor assumption of frozen turbulence have been developed [1, 22–24]. In particular, such last hypothesis amounts to simplify the momentum conservation equations of the NS system by means of pure linear convection, taking as convective velocity the time-averaged velocity field. As a result, for the purpose of inflow conditions generation, the NS equations are usually simplified into linear convection equations with the addition of the divergence-free constraint. This allows to ensure the mathematical treatability needed to arrive to simple analytical solutions, which are highly desirable for the purpose of inflow generation. We remark that the fulfillment of Taylor assumption not only is important in order to avoid pressure fluctuations but it is actually fundamental in order to obtain a correct propagation of the turbulent fluctuations within the computational domain [24]. Additional difficulties arise in the generation of inhomogeneous inflows for which an approximate fulfillment of the divergence-free condition and Taylor assumption is easily obtained while their strict fulfilment is usually remarkably complex (see for instance [25]).

As a result, depending on the adopted synthetic turbulence generation technique, the produced field may or may not fulfill the divergence-free condition and/or Taylor assumption. The fulfillment of the BCs is not usually accommodated in the synthetic field generation method. In such conditions, it is desirable to develop a correction procedure which acts as an interface between the synthetic flow and the CFD simulation. Such correction procedure should, at each time step, correct the synthetic flow applied at the inflow patch in order to impose the fulfillment of NS and the BCs. Such interface, in essence, should avoid that the aforementioned corrections on the velocity field, which are unavoidable, are operated by the pressure field within the CFD simulation, so producing fictitious pressure fluctuations. A technique aimed at obtaining such an effect has been described in [5], giving credit for the paternity of the method to Shirani et al. [Report TF-15, 1981, Mechanical Engineering Department, Stanford University]. The procedure consists in applying the synthetic

velocity field at cell centres in the proximity of the inflow patch in the predictor step of the pressure-velocity coupling algorithm. This allows to operate the necessary corrections on the velocity field by means of the pressure corrector instead of the final pressure (the method has been applied, for instance, in [26–28])

In this paper, a procedure able to efficiently interface synthetic fields and CFD simulations is presented. The procedure is inspired by the aforementioned technique described by Shirani et al. but starts from a radically different perspective. In fact, the method is rationally derived form the Euler approximation of the NS equations and, differently form the aforementioned procedure, allows to insert the inflow velocity as a classical Dirichlet type BC at the inflow patch. No assumption regarding the adopted synthetic turbulence generation method is introduced, so that any one of the available methods can be used. The formulation is derived relying on a variational approach and so, the method is called Variationally Based Inflow Correction method (VBIC).

The paper is organized as follows. Firstly, in Section 2, the origin of pressure fluctuations at the inflow patch is discussed. In Section 3, the VBIC method is presented and numerical results obtained by its application are reported in Section 4. In addition, in Section 5, a general formulation which extends the presented approach, so highlighting its generality, is described. Finally, conclusions are drawn in Section 6.

## 2. The origins of pressure fluctuations

Before proceeding, it is worth to investigate in some detail how pressure fluctuations are generated at the inflow patch by means of simple examples. To this purpose, we analyze a synthetic velocity field characterized by the following form

$$\boldsymbol{u}(\boldsymbol{x},t) = \boldsymbol{U} + \boldsymbol{p}\ \cos(\boldsymbol{k}^T\boldsymbol{x} + \omega t), \tag{2.1}$$

where $\boldsymbol{u}$ represents the unsteady velocity field, $\boldsymbol{U}$ is its time average while $\boldsymbol{p}$ is a vector collecting the amplitudes of the velocity fluctuations. Such fluctuations are modulated by means of the wavevector, $\boldsymbol{k}$, and the angular frequency, $\omega$ while $\boldsymbol{x}$ is the position vector and $t$ denotes time. As already stated, the trace of the velocity field described by Eq. (2.1) on the inflow patch is used as Dirichlet type inflow boundary condition for the CFD simulation, at each time step.

We notice that the velocity fluctuations reported in Eq. (2.1) are the building blocks (hereinafter denoted as velocity waves) used in the generation of synthetic turbulence when spectral methods are adopted. In particular, when a superposition of velocity waves is considered and out of phase terms are introduced, we obtain the four-dimensional Fourier decomposition of the fluctuating velocity field. This implies that, limiting to linear terms, the considerations made in the following can be applied to any velocity field, seen as a superposition of velocity waves.

In the next sections, two aspects are separately discussed in order to isolate the phenomena which lead to the insurgence of pressure fluctuations: the differential properties of the synthetic field and the presence of boundary conditions. The effects induced by the discretization of the governing equations are disregarded and we assume that the structures present in the synthetic field can be well reproduced by the adopted computational grid in space and time. In the following it will be assumed that the time-averaged velocity field is homogeneous and, without loss of generality, that $\boldsymbol{U}$ is directed in the $x_1$ direction and has magnitude $U$. No units of measure are reported and any consistent system of units might be adopted. Simulations shown in this and next sections were performed in OpenFoam 6.0.

### *2.1. Differential properties*

The effects induced by the differential properties of the synthetic field applied to the inflow patch have been already analyzed in [24] in which a new spectral method denoted as PRFG$^3$ has been presented. Here only concepts useful for the present investigation are briefly recalled and the interested reader is invited to refer to [24, 29] for further details. In particular, it is well known that, in order to satisfy the divergence-free condition, $\boldsymbol{p}$ and $\boldsymbol{k}$ must be orthogonal to each other [30] while, in order to fulfill Taylor assumption of frozen turbulence, which will be later further discussed, $k_1 = -\omega/U$, being $k_1$ the first component of the vector $\boldsymbol{k}$. Only if such properties are satisfied, the synthetic field will be correctly transmitted inside the computational domain, so intending that the flow field immediately downstream the patch in the CFD

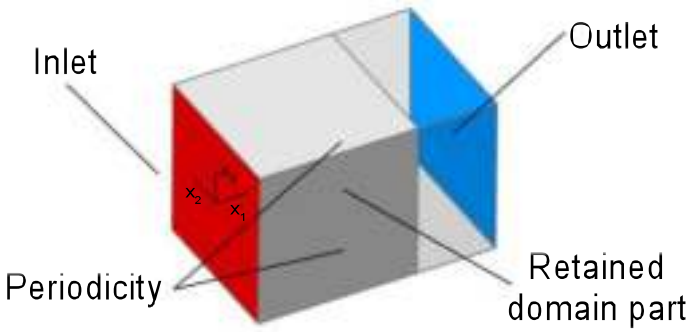


Figure 1: Domain adopted to study the single velocity wave transmission and adopted boundary conditions. Image taken from [24].

simulation will coincide with the synthetic field in the same location. In particular, in order to investigate such aspects, three velocity waves were investigated in [24]:

- **Inflow 1** is a divergence-free velocity wave which respects Taylor assumption: $\omega = -2\pi$, $\boldsymbol{k} = (2\pi, -2\pi, -2\pi)$, $\boldsymbol{p} = (U/10, U/20, U/20)$;
- **Inflow 2** is not divergence-free but Taylor assumption is preserved: $\omega = -2\pi$, $\boldsymbol{k} = (2\pi, -2\pi, -2\pi)$, $\boldsymbol{p} = (U/10, 0, 0)$;
- **Inflow 3** is divergence-free but does not respect Taylor assumption: $\omega = -\pi$, $\boldsymbol{k} = (2\pi, -2\pi, -2\pi)$, $\boldsymbol{p} = (U/10, U/20, U/20)$.

Such synthetic velocity fields were applied to a computational domain of cross-wind dimensions equal to 2 and along-wind dimension equal to 3. The cross-wind dimensions were chosen in order to be a multiple of the wavelengths in the cross-wind directions. In this way, it was possible to apply periodic boundary conditions to all the sides of the computational domain, so avoiding incompatibilities between the velocity fields applied at the inflow and at the sides of the domain.

An overview of the computational domain is provided in Fig. 1. The adopted mesh was completely structured and consisted in hexahedral cells of side 0.02. Time step was set equal to 0.02, leading to a Courant number approximately equal to 1. Unit density, $\rho$, was assumed and simulations run for 10 time units. Only the frontal part of the cube for a length equal to 2 is shown in the following in order to avoid as much as possible to observe effects (not of interest and extremely limited) of the outlet boundary condition.

As expected, only *Inflow 1* is transmitted almost unaltered from the inflow patch to the computational domain. In all other cases, i.e. *Inflow 2* and *Inflow 3*, the velocity field is strongly modified by the pressure filed leading to the insurgence of pressure fluctuations (see Fig. 2). Denoting as $p$ the pressure and as $c_p = p/(1/2\rho U^2)$ the pressure coefficient, it was found that

$$\tilde{c}_p \approx \frac{1}{2}\frac{|(k_\omega p_1/U - k_2 p_2/U - k_3 p_3/U)|}{\sqrt{k_2^2 + k_3^2}}, \tag{2.2}$$

where $\tilde{c}_p$ denotes the amplitude of the pressure coefficient fluctuations and $k_\omega = \omega/U$. Notice that such equation predicts null pressure fluctuations when the divergence-free condition and Taylor assumption are fulfilled. It can be shown that the space derivative in the along wind direction appearing in the divergence-free constraint cannot be generally calculated relying on the synthetic field and, instead, might be better approximated relying on Taylor assumption. In other words, the along-wind space derivatives appearing in the divergence-free constraint should be approximated by means of time derivatives, taking into account the convective velocity. Such aspect has been often overlooked in the development of spectral methods, so explaining some of the difficulties encountered in their use [31, 32]. If the technique used to generate

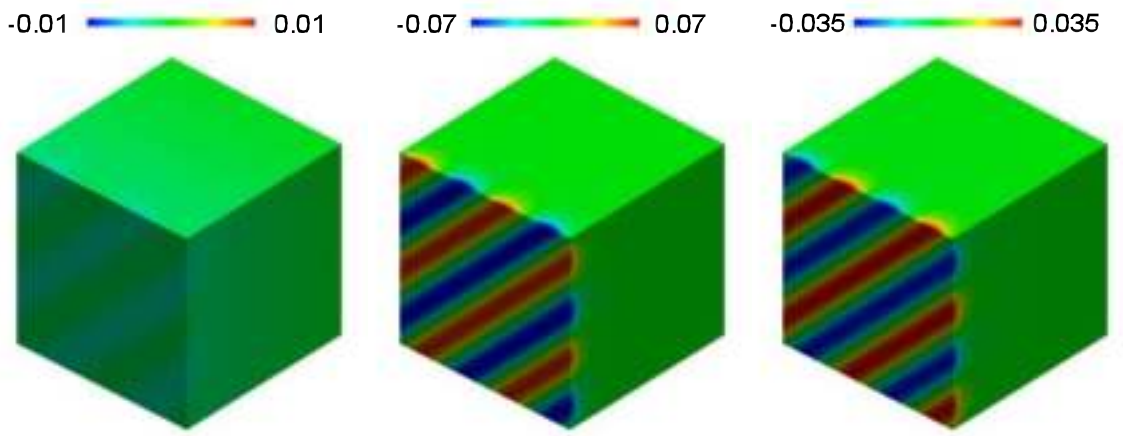


(a) (b) (c)

Figure 2: Pressure fields, $p/\rho$, at $t = 10$: (a) *Inflow 1*, (b) *Inflow 2*, (c) *Inflow 3*. Image taken from [24].

the synthetic field imposes Taylor assumption, the correct relation between space and time derivative is imposed so that along-wind space derivatives in the CFD simulation just downstream the inflow patch can be correctly calculated relying on the synthetic field.

*2.2. Boundary conditions*

We now proceed at investigating the effect induced by the presence of boundary conditions which confine with the inflow patch. In this case we keep the same numerical settings used in the previous section but we change the side patches from periodic to symmetry in order to prevent mass fluxes from the sides. The introduction of symmetry boundary conditions leads to an incompatibility between the lateral BCs and the velocity field applied at the inflow patch, hereinafter denoted as BCs mismatch. The following cases are analyzed

- **Inflow 4** same as *Inflow 1* but with BCs mismatch
  $\omega = -2\pi$, $\boldsymbol{k} = (2\pi, -2\pi, -2\pi)$, $\boldsymbol{p} = (U/10, U/20, U/20)$;
- **Inflow 5** divergence-free and respects Taylor assumption, velocity wave contained in the $x_1 - x_2$ plane and with BCs mismatch:
  $\omega = -2\pi$, $\boldsymbol{k} = (2\pi, -2\pi, 0)$, $\boldsymbol{p} = (U/10, U/10, 0)$.

Figure 3 provides contours of the pressure fluctuations caused by the two inflows, represented by plotting contours of the logarithm of $\sigma^2(p/\rho)$, being $\sigma^2(\cdot)$ the variance. In particular, in Fig. 3 (a), we can see that *Inflow 4* produces pressure fluctuations at the boundaries, as expected. Pressure fluctuations concentrate at the edge and the corners, while, as the applied inflow is divergence-free, the centre of the inflow patch appears to be free from spurious fluctuations. As it will be shown in Sec. 4, the amplitude of the pressure fluctuations in this case is approximately equal to 0.18, corresponding to almost half of the dynamic pressure, which is an extremely high and usually unacceptable value.

Figure 3 (b) shows the pressure fluctuations distribution due to the application of *Inflow 5*. In this case, the maximum amplitude of the fluctuations is approximately equal to 0.3. Although the use of the logarithmic scale surely highlights such effects, whose magnitude notably decreases moving away from the inflow, it clearly shows that a wrong application of inflow conditions can cause strong pressure fluctuations which propagate inside the computational domain for a considerable distance (fluctuations usually decay at a distance from the inflow patch at least comparable to the turbulence integral length scale [2]). The VBIC method is conceived in order to correct the velocity field prior to its application in order to drastically reduce the amplitude of such undesired fictitious pressure fluctuations.

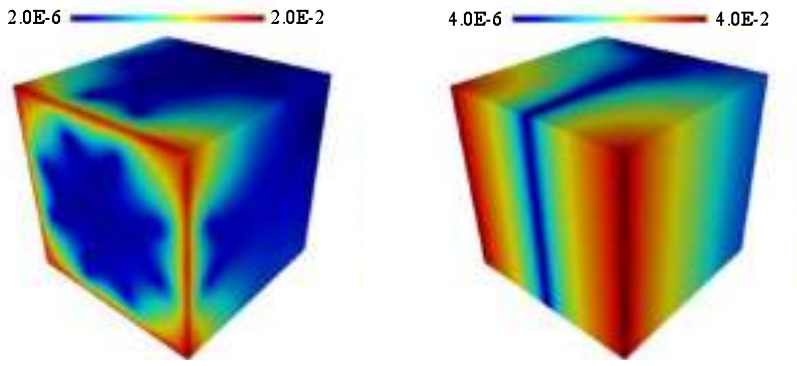


(a) (b)

Figure 3: Contours of $\log_{10}(\sigma^2(p/\rho))$ for: (a) *Inflow 4* and (b) *Inflow 5*.

## 3. The VBIC method

We now proceed to the development of the Variationally Based Inflow Correction (VBIC) method. We assume to apply a time-varying Dirichlet type BC for the velocity field at the inflow patch. As already discussed, we need to ensure that the applied velocity field does not lead to undesired pressure fluctuations due to mass imbalances. A schematic view of an infinitesimal control volume (not to be confused with the finite volumes used for discretization purposes), whose left side is composed by the inflow patch, is shown in Fig. 4. It is worth to point out that, in the following, we will always denote the inflow BC simply as inflow while the term BC will be reserved for the other BCs of the CFD computational domain, which share at least one side with the inflow patch.

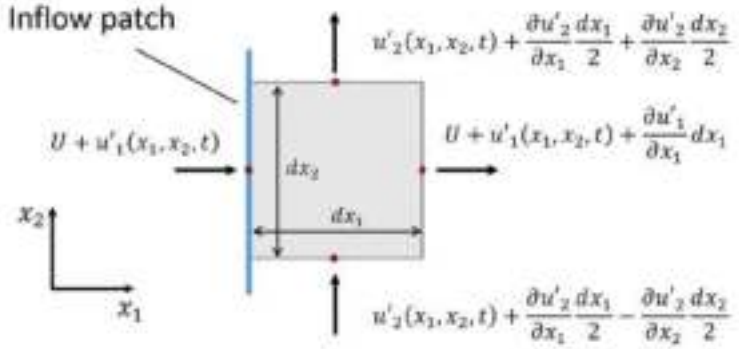


Figure 4: Example of mass fluxes for an infinitesimal control volume located downstream the inflow patch (such figure might be seen as an horizontal slice of Fig. 1 downstream the inflow patch).

We consider an Euler type inviscid and incompressible fluid, so that momentum conservation equations read

$$\frac{\partial u_i}{\partial t}+\frac{\partial u_i}{\partial x_j}u_j+\frac{\partial p}{\rho\partial x_i}=0, \tag{3.1}$$

where $\rho$ is the fluid density and $i,j=1,2,3$. Taking into consideration the along wind momentum conservation equation, the pressure gradient term is set equal to zero in agreement with the usual BC adopted for the pressure field at inflow patches, leading to

$$\frac{\partial u_1}{\partial t}+\frac{\partial u_1}{\partial x_j}u_j=0. \tag{3.2}$$

We decompose the velocity field in its time-averaged component $U$ (directed along the $x_1$ direction), and a fluctuating component, denoted as $\boldsymbol{u}'$. This allows to rewrite Eq. (3.2) as

$$\frac{\partial(U+u_1')}{\partial x_1} = -\frac{1}{U+u_1'}\left[\frac{\partial(U+u_1')}{\partial t} + \frac{\partial(U+u_1')}{\partial x_2}u_2' + \frac{\partial(U+u_1')}{\partial x_3}u_3'\right], \tag{3.3}$$

which, assuming that the time-averaged field is homogeneous or slowly varying, can be simplified as

$$\frac{\partial u_1'}{\partial x_1} \approx -\frac{1}{U+u_1'}\left[\frac{\partial u_1'}{\partial t} + \frac{\partial u_1'}{\partial x_2}u_2' + \frac{\partial u_1'}{\partial x_3}u_3'\right], \tag{3.4}$$

Assuming small values for the primed quantities and for their derivatives, leads to

$$\frac{\partial u_1'}{\partial x_1} \approx -\frac{1}{U+u_1'}\left[\frac{\partial u_1'}{\partial t}\right]. \tag{3.5}$$

The along-wind-directed momentum conservation equation, in the form presented in Eq. (3.5), represents the starting point of the VBIC method (Eq. (3.3) might be also used to this purpose when the situation suggests that some of the disregarded terms might be of considerable importance).

**Remark 1:** Starting from Eq. (3.5) and disregarding $u_1'$ with respect to $U$ leads to

$$\frac{\partial u_1'}{\partial x_1} \approx -\frac{1}{U}\frac{\partial u_1'}{\partial t}, \tag{3.6}$$

which is the classical approximation of Euler equations based on linear convection, often denoted as Taylor assumption.

**Remark 2:** The possibility to disregard derivatives of the primed quantities is not immediately obvious. In particular, despite the smallness of the primed quantities, their derivatives might be large. Nevertheless, such behavior has to be attributed to localized phenomena which are not here of primary interest.

**Remark 3:** The calculation of along wind space derivatives by means of time derivatives using the momentum conservation equation is straightforward from the analytical point of view but might fall short in a discrete framework. This might be particularly problematic if time and space resolutions are remarkably different. From now on we will assume that turbulent fluctuations are well represented in both space and time. In practice, this means that high-frequency contributions which cannot be properly represented by the grid in space and/or time should be filtered away before being imputed into the VBIC procedure. As such contributions would be anyway quickly dissipated in the CFD simulation, this does not appear to be a problem of primary importance.

Figure 4 shows the velocities at the faces of an infinitesimal control volume located downstream the inflow patch, calculated by means of a first order Taylor expansion. We notice that the neat mass flux entering the control volume due to the time-averaged velocity component is null, as it has been assumed to be homogeneous in the along wind direction. As a result, from now on, we concentrate only on the primed quantities and, for the sake of notation simplicity, we omit the prime symbol. Mass conservation thus requires

$$\frac{\partial u_1}{\partial x_1} + \frac{\partial u_2}{\partial x_2} + \frac{\partial u_3}{\partial x_3} = 0. \tag{3.7}$$

Substituting Eq. (3.5) into Eq. (3.7), it is possible to write

$$-\frac{1}{U+u_1}\frac{\partial u_1}{\partial t} + \frac{\partial u_2}{\partial x_2} + \frac{\partial u_3}{\partial x_3} = 0. \tag{3.8}$$

*3.1. Velocity field correction*

We now consider that the fluctuating velocity field to be applied at the inflow patch, $\boldsymbol{u}$, is actually decomposed into two contributions

$$\boldsymbol{u} = \boldsymbol{u}^s + \boldsymbol{u}^c, \tag{3.9}$$

where $\boldsymbol{u}^s$ is a known synthetically generated velocity field while $\boldsymbol{u}^c$ is an unknown correction to be calculated at each time-step, in order to prevent mass imbalances. We assume $\boldsymbol{u}^c$ to have the following form

$$\boldsymbol{u}^c = [0, u_2^c, u_3^c], \tag{3.10}$$

which shows that the correction of the along-wind velocity component has been assumed to be identically null. Such choice, arbitrary in nature, is related to the fact that correcting all three velocity components notably complicates the formulation which, instead, is here presented in its simplest form (further details on such aspect can be found in Section 5).

The correction $\boldsymbol{u}^c$ is conceived in order to impose the divergence-free condition and avoid BCs mismatches, taking into account Eq. (3.5). In particular, we want $\boldsymbol{u}^c$ to be minimal in order to have $\boldsymbol{u} \approx \boldsymbol{u}^s$. In the traditional framework of variational calculus, assuming $\Omega$ to be the inflow patch, we write

$$I = \int_\Omega \mathcal{L} \, \mathrm{d}\Omega, \tag{3.11}$$

where

$$\mathcal{L} = (u_2^c)^2 + (u_3^c)^2 + 2\lambda \left[ -\frac{1}{U + u_1} \frac{\partial u_1}{\partial t} + \frac{\partial u_2}{\partial x_2} + \frac{\partial u_3}{\partial x_3} \right]. \tag{3.12}$$

The first part of $\mathcal{L}$ represents the $L2$ norm of the correction over the patch and ensures that the correction is minimal in the $L2$ sense (so ensuring its smallness) while the second part is the imposition of the divergence-free condition, in the form provided by Eq. (3.8), by means of a Lagrange multiplier, $2\lambda$. We further stress that, as regards the present investigation, the velocity field is defined only at the inflow patch and, consequently, the integral $I$ appearing in Eq. (3.11) is calculated on the two-dimensional domain of the inflow patch. Such expression, taking into account Eq. (3.9), can be rewritten as

$$\mathcal{L} = (u_2^c)^2 + (u_3^c)^2 + 2\lambda \left[ -\frac{1}{U + u_1^s} \frac{\partial u_1^s}{\partial t} + \frac{\partial (u_2^s + u_2^c)}{\partial x_2} + \frac{\partial (u_3^s + u_3^c)}{\partial x_3} \right]. \tag{3.13}$$

We can highlight the unknown terms and collect all the known ones leading to

$$\mathcal{L} = (u_2^c)^2 + (u_3^c)^2 + 2\lambda \left( \frac{\partial u_2^c}{\partial x_2} + \frac{\partial u_3^c}{\partial x_3} - R \right), \tag{3.14}$$

where $R$ is

$$R = \frac{1}{U + u_1^s} \frac{\partial u_1^s}{\partial t} - \frac{\partial u_2^s}{\partial x_2} - \frac{\partial u_3^s}{\partial x_3}. \tag{3.15}$$

The minimization of $I$ is classically performed writing the corresponding Euler-Lagrange equations. In particular, the unknown fields, $q_k$, are the two components of the velocity correction $\boldsymbol{u^c}$ and the Lagrange multiplier $2\lambda$. The Euler-Lagrange equations are calculated as

$$\frac{\partial \mathcal{L}}{\partial q_k} - \sum_i \frac{\partial}{\partial x_i} \left( \frac{\partial \mathcal{L}}{\partial q_{k,i}} \right) = 0, \tag{3.16}$$

where $q_{k,i}$ denotes the derivative of $q_k$ in the $i-$th spatial direction. The Euler-Lagrange equations thus read

$$\begin{cases} u_2^c - \frac{\partial \lambda}{\partial x_2} = 0 \\ u_3^c - \frac{\partial \lambda}{\partial x_3} = 0 \\ \frac{\partial u_2^c}{\partial x_2} + \frac{\partial u_3^c}{\partial x_3} - R = 0. \end{cases} \tag{3.17}$$

Substituting the first two of Eq. (3.17) into the last one, we obtain

$$\nabla^2 \lambda = R, \tag{3.18}$$

which must be solved on the two-dimensional domain of the inflow patch in order to evaluate the velocity corrections. The result is indeed expected: in order to have minimal norm the rotational part of the velocity correction field must be null as it would not contribute to compensate the divergence introduced by the synthetic field, $R$. As it is well known, the irrationality of the corrections leads to the existence of their potential, $\lambda$.

The BCs to be applied to Eq. (3.18) at the inflow patch boundaries should be such to prevent fluxes which cannot be realised due to the presence of other BCs of the computational domain (e.g. symmetry, periodicity, walls, etc). For example, let us assume that the inflow patch, normal to the $x_1$ direction, confines with a symmetry condition normal to the $x_2$ direction. In such case, at the line of intersection between the two patches (i.e. inflow and symmetry), corrections should be such to completely suppress $u_2$ velocity fluctuations (i.e. $u_2^c = -u_2^s$). This leads to the imposition of Neumann type BCs to the problem described by Eq. (3.18). In fact, according to the first and second of Eq. (3.17) at the inflow patch boundary

$$u_2^c = \frac{\partial \lambda}{\partial x_2} = -u_2^s. \tag{3.19}$$

Notice that, in order to impose null normal velocities on the whole boundary, the problem described by Eq. (3.18) must be solved when only Neumann type BCs are imposed. This problem is analogous to the solution of the pressure equation solved by pressure-velocity coupling algorithms when no Dirichlet BC is imposed on the pressure field. It is well known that such problem has solution only if the sources and boundary fluxes compensate exactly. In our case this means that the integral of the divergence of the synthetic field and the boundary fluxes must compensate exactly. Other types of BCs, different from symmetry, lead to identical considerations. From the operative point of view it is thus necessary to enforce that the known term of the discretized version of Eq. (3.18) sum to zero, which substantially leads to a uniform redistribution of the global mass imbalance over the entire patch. Such mass imbalance can be actually compensated by subtracting from $u_1^s$ its mean value over the patch, so that the total mass flux entering the domain is constant and equal to that provided by the time-average velocity field [1]. Overall such operation is expected to lead to very small effects in the majority of the cases and has been adopted in obtaining the following numerical results. We remark again that, despite some similarities, the VBIC procedure should not be confused with pressure-velocity coupling algorithms used to impose the divergence-free condition inside the computational domain when segregated solution schemes are adopted.

**Remark 4:** The minimization of Eq. (3.11) can be performed by following the well-known procedure developed by Lagrange. In particular, taking into consideration Eq. (3.14), Eq. (3.11) can be rewritten as $I(u_2^c, u_3^c, \lambda)$. The stationarity of such functional, after simple algebraic manipulations, leads to the system of Eq. (3.17), complemented by the boundary term

$$\int_{\partial\Omega} \lambda \boldsymbol{\delta u^c} \cdot \boldsymbol{n} \mathrm{d}(\partial\Omega) = 0, \tag{3.20}$$

where $\partial\Omega$ is the boundary of the inflow patch and $\boldsymbol{n}$ is its outward-pointing normal. When normal velocity corrections are imposed at the inflow patch boundary, their variations must be there null and Eq. (3.19) is recovered while, in case of free velocities, Eq. (3.20) requires to impose a null value for the velocity potential $\lambda$.

## 4. Numerical results

In this section we present numerical results obtained by applying the VBIC method. To this purpose we analyze again *Inflow 4* and *Inflow 5* to which we add two more general inflows denoted as *Inflow 6* and *Inflow 7*.

*Inflow 6* is characterized by a non-homogeneous distribution of the time-averaged velocity field such that

$$U(x_3) = 1 + x_3/2. \tag{4.1}$$

In this case, the velocity fluctuations are prescribed as the semi-sum of that of *Inflow 4* and *Inflow 5*. Notice that the inhomogeneity of the velocity field substantially introduces a violation of Taylor assumption which is in fact fulfilled only for $x_3 = 0$ (located at the centre of the cube).

*Inflow 7* is built in order to provide a complete overview of the procedure potential. Despite its simplicity, it is in fact well representative of turbulence generated by superposition of velocity waves and, as any velocity field can be expressed by means of a Fourier expansion, it is representative of any synthetic velocity field, regardless of the particular method used to generate it. In particular, we consider a superposition of velocity waves such that their wavevectors are

$$\boldsymbol{k}_1 = (-1.25, -1.25, 0.0), \quad \boldsymbol{k}_2 = (2.25, 1.50, 0.75), \quad \boldsymbol{k}_3 = (-1.0, -2.25, 1.25), \quad \boldsymbol{k}_4 = (0.5, -1.75, 2.25), \tag{4.2}$$

while the amplitude vector is the same for all the velocity waves and equal to $\boldsymbol{p} = (0.5, 0.5, 0.5)$. Taylor assumption is fulfilled imposing $\omega_i = -k_{1i}U$ for each $i$-th velocity wave with $i = 1, 2, 3, 4$. The time-averaged velocity magnitude is equal to 10. For each velocity component the sum of the amplitudes of all velocity waves is equal to 2.0. It can be noticed that the synthetic flow field is not divergence-free ($\boldsymbol{k}_i$ and $\boldsymbol{p}$ are not orthogonal) so that strong pressure fluctuations can be expected. Such configuration will be denoted as *Inflow 7A*. By changing the sign of all first components of the wavevectors, we obtain a divergence-free inflow (characterized by the same spectral content), which we denote *Inflow 7B*. In this case pressure fluctuations are expected only due to boundary conditions mismatching.

The numerical solution of Eq. (3.18) has been obtained by means of standard linear quadrangular finite elements which follows the finite volume discretization adopted for the CFD simulation.

### *4.1. Inflow 4*

The flow field obtained for *Inflow 4* when no correction is applied to the velocity field is reported in Fig. 5. In particular, the strong pressure fluctuations produced at the inflow patch boundaries can be observed as already commented in Fig. 3 (a). At the edges such pressure fluctuations are characterized by amplitude equal to approximately 0.1, which is a remarkable value if compared to the dynamic pressure calculated based on the time-averaged velocity (the dynamic pressure is equal to 0.5 in this case). At the corners such value is almost doubled. Notice that the actual extreme values are reported in parentheses under the figure color bar while the color bar range has been fixed in order to allow an easy comparison between uncorrected and corrected cases. Figure 5 (c) and Figure 5 (d) show the damping effect operated by the symmetry BCs on the corresponding orthogonal velocity component, as expected. Notice that the depicted values are calculated at the cell centres, not face centres, so that velocity components normal to the symmetry BCs are not expected to be exactly null. As expected the $u_1$ velocity component appears to be modified, exceeding the expected range of variation (expected to be equal to 1/10 for $u_1$ and 1/20 for $u_2$ and $u_3$) as it contributes to compensate for the mass imbalances produced by the mismatching BCs.

Looking now at Fig. 6, it is possible to observe that the amplitude of the pressure fluctuations decreases of one order of magnitude when the VBIC method is applied in order to correct the velocity field before applying it to the inflow patch. The distribution of the $u_1$ velocity component matches the one expected from the synthetic field in the proximity of the inflow patch, which leads to an almost perfect matching of the range of variation for $u_1$ (see Fig. 6 (b)). Such result is indeed expected as VBIC does not apply corrections to the $u_1$ velocity component, in agreement with Eq. (3.10). On the other side, apparent modifications of the $u_2$ and $u_3$ velocity components can be observed: the incompatibility of the inflow velocity field with the symmetry conditions applied on the sides has been removed by the VBIC method as shown in Fig. 6 (c) and Fig. 6 (d). By construction, the applied corrections have minimal $L2$ norm over the inflow patch.

### *4.2. Inflow 5*

Figure 7 reports the results obtained for *Inflow 5* when no corrections are applied while Fig. 8 reports the results obtained by means of the VBIC method. Overall, results observed for the *Inflow 4* are confirmed.

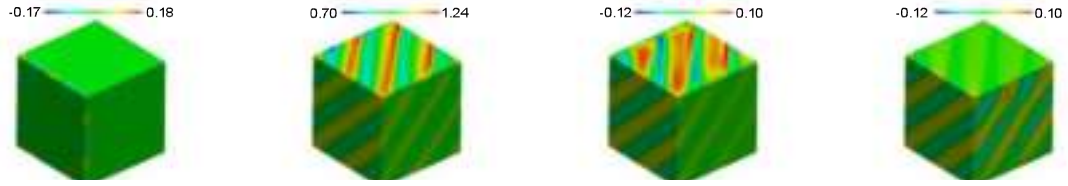


(a) (b) (c) (d)

Figure 5: Flow field for *Inflow 4* at $t = 10$, no correction applied: (a) $p/\rho$, (b) $u_1$, (c) $u_2$ and (d) $u_3$.

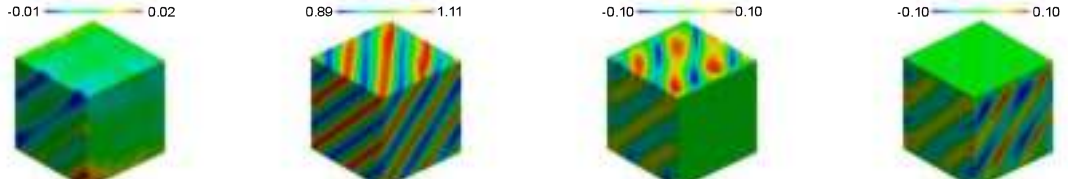


(a) (b) (c) (d)

Figure 6: Flow field for *Inflow 4* at $t = 10$, corrections applied: (a) $p/\rho$, (b) $u_1$, (c) $u_2$ and (d) $u_3$.

Pressure fluctuations decrease of one order of magnitude when corrections are applied. In this case, due to the absence of the $u_3$ velocity component and the symmetry of the problem, the mass surplus/deficits introduced by the mismatching BCs are compensated by the $u_1$ and $u_2$ velocity components for the uncorrected field and by the $u_2$ velocity component only for the corrected field. This explains the fact that the peak value of the $u_2$ velocity fluctuations is approximately doubled with respect to the expected one when corrections are applied while smaller differences are observed for the uncorrected case.

### *4.3. Inflow 6*

Figure 9 and Figure 10 report the results obtained for *Inflow 6* without and with applied corrections, respectively. Also in this case pressure fluctuations are decreased of one order of magnitude in agreement with the previously presented tests. Notice that in this case the applied inflow is actually not divergence-free as the time-averaged velocity varies with the $x_3$ coordinates, so that Taylor assumption is respected only for $x_3 = 0$. As already discussed, the imposition of the divergence-free condition on the synthetic field does not correspond to its imposition over the transmitted velocity field when Taylor assumption is not fulfilled. Despite such observation, the strongest pressure fluctuations are still observed in the proximity of the inflow patch boundaries. Notice also that in the bottom part of the domain (i.e. for $x_3 = -1$) the amplitude of the $u_1$ velocity component is equal to 20% of the time-averaged velocity magnitude.

### *4.4. Inflow 7*

Figure 11 reports the results obtained for *Inflow 7A* at $t = 1$ (the total time and the time steps have been decreased of a factor 10 because the time-averaged velocity magnitude has been increased of the same factor). Strong pressure fluctuations are generated over all the inflow patch in order to compensate for mass imbalances as the inflow is not divergence-free. In this case, the maximum amplitude of such pressure fluctuations well exceeds 50% of the dynamic pressure value. Looking now at Fig. 12, which corresponds to the divergence-free version of *Inflow 7A*, namely *Inflow 7B*, pressure fluctuations are concentrated at the edges of the inflow patch, as expected. Finally, the results obtained with *Inflow 7A* when the VBIC method is adopted are shown in Fig. 13 (for the sake of conciseness the corrected case for *Inflow 7B* is not shown as it would be redundant). As in the previous case pressure fluctuations at the inflow patch substantially decrease assuming values which, although slightly higher, appear to be compatible with that recorded in the flow field downstream the inflow patch, as shown in Fig. 13 (a). Notice that the proposed procedure is in no way expected to provide null pressure fluctuations as only the along wind pressure gradient component

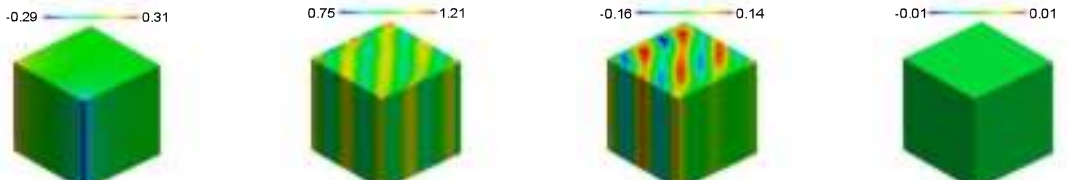


(a) (b) (c) (d)

Figure 7: Flow field for *Inflow 5* at $t = 10$, no correction applied: (a) $p/\rho$, (b) $u_1$, (c) $u_2$ and (d) $u_3$.

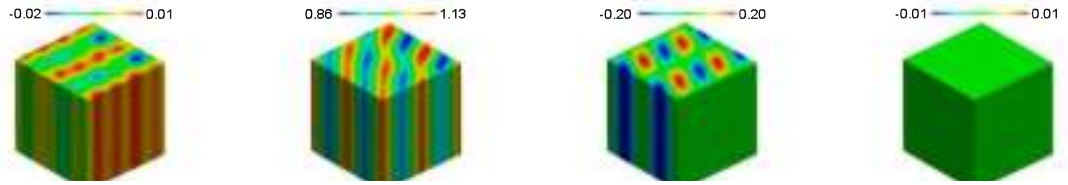


(a) (b) (c) (d)

Figure 8: Flow field for *Inflow 5* at $t = 10$, corrections applied: (a) $p/\rho$, (b) $u_1$, (c) $u_2$ and (d) $u_3$.

is restraint to a null value. Simply, pressure fluctuations are expected to be comparable to that observed in the free-field, as confirmed by the proposed numerical tests.

## 5. A general formulation

In this section we develop a more general formulation in which the along-wind velocity component is considered in the minimization process. In other words, we modify Eq. (3.10) in order to consider non null $u_1^c$. Such formulation leads to nonlinear terms which would require appropriate treatment. Due to such complications, the formulation is here presented only from the theoretical point of view in order to provide a complete picture of the matter for the interested reader. The presented developments allow also to appreciate the generality of the approach as well as paving the way to other extensions. In particular, taking into account corrections for the $u_1$ velocity components, the Lagrangian previously reported in Eq. (3.12) reads

$$\mathcal{L} = (u_1^c)^2 + (u_2^c)^2 + (u_3^c)^2 + \lambda \left[ -\frac{1}{U + u_1^s + u_1^c} \frac{\partial (u_1^s + u_1^c)}{\partial t} + \frac{\partial (u_2^s + u_2^c)}{\partial x_2} + \frac{\partial (u_3^s + u_3^c)}{\partial x_3} \right]. \tag{5.1}$$

In the following we assume to approximate the term $U + u_1^s + u_1^c$ in an explicit way and denote it as $u^*$ (known at the current time step). We point out that such approximation might be also seen as the starting point of an iterative correction procedure. With such approximation we can rewrite Eq. (5.1) as

$$\mathcal{L} = (u_1^c)^2 + (u_2^c)^2 + (u_3^c)^2 + \lambda \left( -\frac{1}{u^*} \frac{\partial (u_1^s + u_1^c)}{\partial t} + \frac{\partial (u_2^s + u_2^c)}{\partial x_2} + \frac{\partial (u_3^s + u_3^c)}{\partial x_3} \right). \tag{5.2}$$

It is now necessary to approximate the time derivatives in order to obtain a solution in a semi-discrete framework, in analogy to the approach usually followed by CFD solvers. In particular, using a backward Euler scheme, we can write

$$\frac{1}{u^*} \frac{\partial (u_1^s + u_1^c)}{\partial t} \approx \frac{1}{u^*} \frac{u_1^s + u_1^c - u_1^{s,old} - u_1^{c,old}}{\Delta t} = \frac{1}{u^*} \frac{u_1^s + u_1^c - u_1^{old}}{\Delta t}, \tag{5.3}$$

where quantities marked as *old* are evaluated at the previous time step. Notice that any other implicit time discretization method might be used in such passage. Introducing Eq. (5.3) into Eq. (5.2), it is possible to

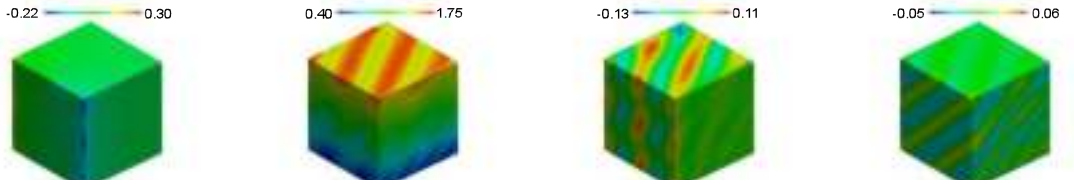


(a) (b) (c) (d)

Figure 9: Flow field for *Inflow 6* at $t = 10$, no correction applied: (a) $p/\rho$, (b) $u_1$, (c) $u_2$ and (d) $u_3$.

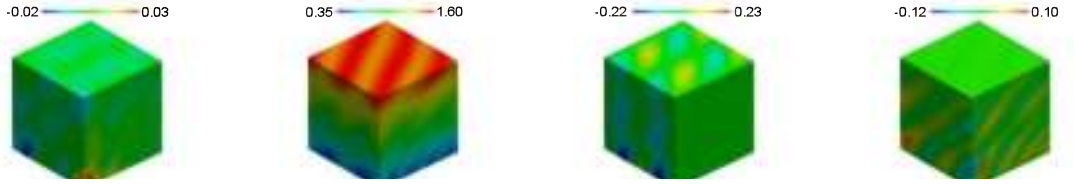


(a) (b) (c) (d)

Figure 10: Flow field for *Inflow 6* at $t = 10$, corrections applied: (a) $p/\rho$, (b) $u_1$, (c) $u_2$ and (d) $u_3$.

write

$$\mathcal{L} = (u_1^c)^2 + (u_2^c)^2 + (u_3^c)^2 + \lambda \left( -\frac{1}{u^*} \frac{u_1^c}{\Delta t} + \frac{\partial u_2^c}{\partial x_2} + \frac{\partial u_3^c}{\partial x_3} - R \right), \tag{5.4}$$

where $R$ is

$$R = \frac{1}{u^* \Delta t} \left( u_1^s - u_1^{old} \right) - \frac{\partial u_2^s}{\partial x_2} - \frac{\partial u_3^s}{\partial x_3}. \tag{5.5}$$

The Euler-Lagrange equations now read

$$\begin{cases} 2u_1^c - \frac{\lambda}{u^* \Delta t} = 0 \\ 2u_2^c - \frac{\partial \lambda}{\partial x_2} = 0 \\ 2u_3^c - \frac{\partial \lambda}{\partial x_3} = 0 \\ -\frac{u_1^c}{u^* \Delta t} + \frac{\partial u_2^c}{\partial x_2} + \frac{\partial u_3^c}{\partial x_3} - R = 0, \end{cases} \tag{5.6}$$

In particular, from the first of Eqs. (5.6) we obtain

$$\lambda = 2 u_1^c u^* \Delta t, \tag{5.7}$$

which, substituted in the second and third, leads to

$$\begin{aligned} u_2^c &= \Delta t \frac{\partial (u_1^c u^*)}{\partial x_2} = \Delta t \left( \frac{\partial u_1^c}{\partial x_2} u^* + \frac{\partial u^*}{\partial x_2} u_1^c \right), \\ u_3^c &= \Delta t \frac{\partial (u_1^c u^*)}{\partial x_3} = \Delta t \left( \frac{\partial u_1^c}{\partial x_3} u^* + \frac{\partial u^*}{\partial x_3} u_1^c \right). \end{aligned} \tag{5.8}$$

In order to substitute such result into the last of Eq. (5.6), we calculate

$$\frac{\partial u_2^c}{\partial x_2} = \Delta t \left( \frac{\partial^2 u_1^c}{\partial x_2^2} u^* + 2 \frac{\partial u^*}{\partial x_2} \frac{\partial u_1^c}{\partial x_2} + \frac{\partial^2 u^*}{\partial x_2^2} u_1^c \right), \tag{5.9}$$

$$\frac{\partial u_3^c}{\partial x_3} = \Delta t \left( \frac{\partial^2 u_1^c}{\partial x_3^2} u^* + 2 \frac{\partial u^*}{\partial x_3} \frac{\partial u_1^c}{\partial x_3} + \frac{\partial^2 u^*}{\partial x_3^2} u_1^c \right). \tag{5.10}$$

Substituting the previously calculated results in the last of Eqs. (5.6), we obtain

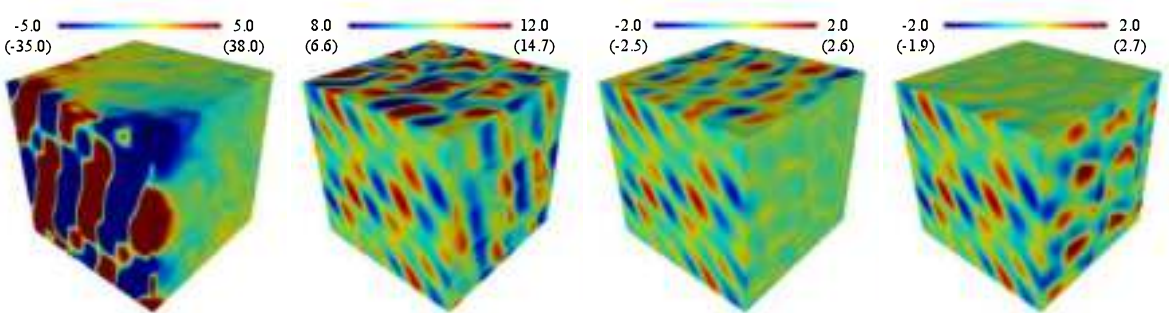


(a) (b) (c) (d)

Figure 11: Flow field for *Inflow 7A* at $t = 1$, no correction applied: (a) $p/\rho$, (b) $u_1$, (c) $u_2$ and (d) $u_3$.

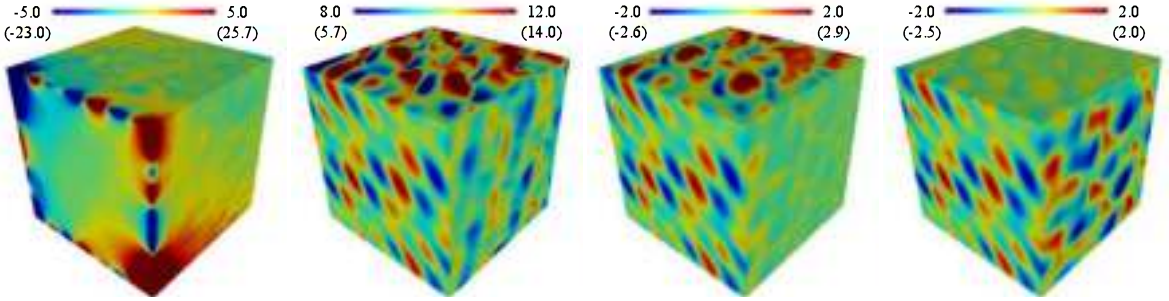


(a) (b) (c) (d)

Figure 12: Flow field for *Inflow 7B* at $t = 1$, no correction applied: (a) $p/\rho$, (b) $u_1$, (c) $u_2$ and (d) $u_3$.

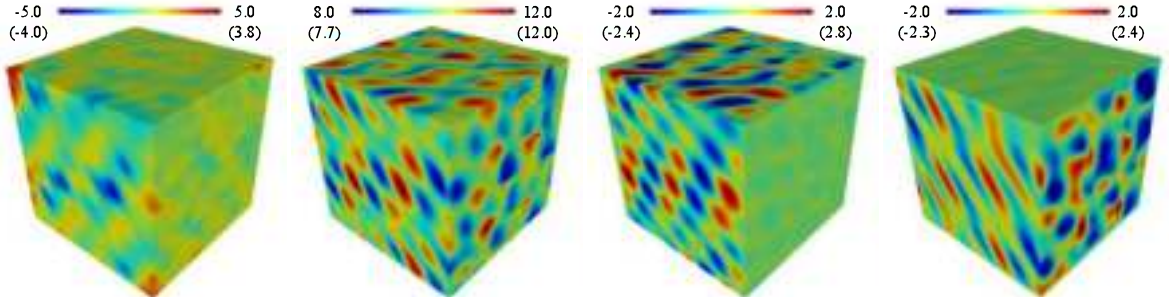


(a) (b) (c) (d)

Figure 13: Flow field for *Inflow 7A* at $t = 1$, correction applied: (a) $p/\rho$, (b) $u_1$, (c) $u_2$ and (d) $u_3$.

$$\frac{\partial^2 u_1^c}{\partial x_2^2} + \frac{\partial^2 u_1^c}{\partial x_3^2} + \frac{2}{u^*}\left(\frac{\partial u^*}{\partial x_2}\frac{\partial u_1^c}{\partial x_2} + \frac{\partial u^*}{\partial x_3}\frac{\partial u_1^c}{\partial x_3}\right) + \frac{u_1^c}{u^*}\left(\frac{\partial^2 u^*}{\partial x_2^2} + \frac{\partial^2 u^*}{\partial x_3^2}\right) - \frac{u_1^c}{(u^*\Delta t)^2} - \frac{R}{u^*\Delta t} = 0, \tag{5.11}$$

which can be also expressed as

$$\nabla^2 u_1^c + \frac{2}{u^*}\nabla u_1^c \cdot \nabla u^* + \frac{u_1^c}{u^*}\left(\nabla^2 u^* - \frac{1}{u^*\Delta t^2}\right) = \frac{R}{u^*\Delta t}, \tag{5.12}$$

while BCs in this case are of mixed type and are provided by

$$u_2^c = \Delta t \left( \frac{\partial u_1^c}{\partial x_2} u^* + \frac{\partial u^*}{\partial x_2} u_1^c \right) = -u_2^s. \tag{5.13}$$

We notice that such general formulation, in the present form, might suffer from the formation of boundary layers, in the proximity of the borders of the inflow patch. This can be deduced by assuming a constant $u^*$ and a mono-dimensional domain. In such conditions, the homogeneous version of Eq. (5.12) becomes

$$\frac{\mathrm{d}^2 u_1^c}{\mathrm{d}x^2} - \frac{u_1^c}{u^{*2}\Delta t^2} = 0, \tag{5.14}$$

which has solutions of the type

$$u_1^c = A e^{+\frac{x}{u^*\Delta t}} + B e^{-\frac{x}{u^*\Delta t}}, \tag{5.15}$$

where the constants $A$ and $B$ must be determined in agreement with the BCs. It can be clearly seen that, following this formulation, corrections are applied on a boundary layer whose thickness vanishes with the time step size, which, although rationally deduced from the minimization of the corrections $L2$ norm over the inflow patch, might be indeed an undesirable feature as it leads to numerical difficulties. Despite such shortcomings, the proposed extension clearly shows the great potential of the VBIC method which, thanks to its variational background, provides a rational framework for the application of unsteady velocity fields as Dirichlet type boundary conditions.

**Remark 5:** It might be noticed that at wall boundaries confining with the inflow patch, it would be necessary to impose null value of the velocity in the normal as well as in the tangential directions with respect to the wall. Such operation would require to impose three velocity components at the same point which, in the current framework, would be impossible as this leads to a mismatch of boundary conditions (impossibility to prescribe the value of $u_1^c$ and mixed type boundary conditions at the same time). Such aspect would be overcome if, instead of using Euler equations in Eq. (3.5), the complete NS equations are used. This would introduce second-order derivatives in space (i.e. viscous terms) in Eq. (3.8) which, once imputed in the variational calculus machinery, would provide forth-order Euler-Lagrange equations, so allowing the contemporaneous imposition of three velocity components on the same BC. This is consistent with the behavior of the Euler and Navier-Stokes equations, respectively.

## 6. Conclusions

In this paper, the problem of interfacing synthetically generated inflow conditions with CFD simulations has been addressed. It has been shown that, in order to avoid undesired pressure fluctuations, the compatibility between the velocity field applied at the inflow patch and that realized inside the computational domain must be carefully considered. Such compatibility must be guaranteed taking into consideration two aspects: the differential properties of the synthetic field and the boundary conditions imposed on patches which confine with the inflow one.

The VBIC method is a procedure which allows to modify arbitrary velocity fields in order to make them suitable for the application as inflow conditions. The methodology is deduced from Euler equations and it is conceived as an interface between the synthetic field and the numerical simulation. The correction strategy is deduced basing on a variational background, so providing a simple yet powerful and rational framework in the formulation development. In its simplest form, the procedure simply requires to solve a Poisson equation onto the two-dimensional space of the inflow patch, at each time step.

Despite its simplicity, the procedure proved to be effective in reducing the pressure fluctuations observed when unsteady velocity fields are applied as inflow conditions and it is amenable to further improvements and extensions. We finally remark that the procedure should not be conceived as an alternative to the development of appropriate synthetic flows as, by applying corrections, VBIC changes the spectral/correlation properties of the applied field. The entity of such modifications generally depend on the synthetic field *a priori* compatibility with the NS equations.

In the authors' opinion, the proposed procedure might be found particularly useful in inhomogeneous flows, which often lead to synthetic fields which are almost divergence-free and/or almost comply with Taylor assumption, and in order to suppress undesired pressure fluctuations caused by boundary conditions mismatches.

## References


[1] R. Poletto, T. Craft, and A. Revell, "A new divergence free synthetic eddy method for the reproduction of inlet flow conditions for LES," *Int Jou Heat Fluid Flow*, vol. 91, pp. 519–539, 2013.

[2] M. Bervida, L. Patruno, S. Stănic, and de Miranda S., "Synthetic generation of the atmospheric boundary layer for wind loading assessment using spectral methods," *Under review.*

[3] T. Saad and J. Sutherland, "Comment on diffusion by a random velocity field," *Physics of Fluids*, vol. 28, pp. 119–101, 2016.

[4] T. Saad, D. Cline, R. Stoll, and J. Sutherland, "Scalable tools for generating synthetic isotropic turbulence with arbitrary spectra," *AIAA Journal*, vol. 55, pp. 327–331, 2017.

[5] K. Kondo and A. Murakami, "Generation of veocity fluctuations for inflow boundary condition of les," *J Wind Eng Ind Aerodyn*, vol. 67&68, pp. 51–64, 1997.

[6] X. Wu, "Inflow turbulence generation methods," *Annual Review of Fluid Mechanics*, vol. 49, pp. 23–49, 2017.

[7] K. Alvelius, "Random forcing of three-dimensional homogeneous turbulence," *Physics of Fluids.*

[8] P. Schlatter and Örlü, "Assessment of direct numerical simulation data of turbulent boundary layers," *Journal of Fluid Mechanics*, vol. 659, pp. 116–126, 2010.

[9] P. Schlatter and Örlü, "Turbulent boundary layers at moderate reynolds numbers: inflow length andtripping effects," *Journal of Fluid Mechanics*, vol. 710, pp. 5–34, 2012.

[10] L. Davidson, "Using isotropic synthetic fluctuations as inlet boundary conditions for unsteady simulations," *Advances and Applications in Fluid Mechanics*, vol. 1, pp. 1–35, 2007.

[11] R. Rogallo and P. Moin, "Numerical simulation of turbulent flows," *Annu. Rev. Fluid Mech.*, vol. 16, pp. 99–137, 1984.

[12] P. Spalart, "Direct numerical simulation of turbulent boundary layer up to $R_\theta = 1410$," *J. Fluid Mech.*, vol. 187, p. 61, 1988.

[13] P. Moin and J. Kim, "Direct numerical simulation: a tool in turbulence research," *Annu. Rev. Fluid Mech.*, vol. 30, pp. 539–558, 1998.

[14] T. Lund, X. Wu, and K. Squires, "Generation of turbulent inflow data for spatially-developing boundary layer simulations," *Journal of Computational Physics*, vol. 140, pp. 233–258, 1998.

[15] T. Helgedagsrud, Y. Bazilevs, K. Mathisen, J. Yan, and O. Øseth, "Modeling and simulation of bridge-section buffeting response in turbulent flow," *Mathematical Models and Methods in Applied Sciences*, vol. 29, pp. 936–966, 2019.

[16] A. Gungor, J. Sillero, and J. Jiménez, "Pressure statistics from direct simulation of turbulent boundary layer," *Seventh International Conference on Computational Fluid Dynamics (ICCFD7), Big Island, Hawaii, July 9-13*, 2012.

[17] A. Smirnov, S. Shi, and I. Celik, "Random flow generation technique for large eddy simulations and particle-dynamics modeling," *Jou Flu Eng*, vol. 123, pp. 359–371, 2001.

[18] M. Klein, A. Sadiki, and J. Janicka, "A digital filter based generation of inflow data for spatially developing direct numerical or large eddy simulations," *Journal of computational Physics*, vol. 186, pp. 652–665, 2003.

[19] N. Jerrin, S. Benhamadouche, D. Laurence, and R. Prosser, "A synthetic-eddy-method for generating inflow conditions for large-eddy simulations," *International Journal of Heat and Fluid Flow*, vol. 27, p. 585593, 2006.

[20] Z. Xie and I. Castro, "Efficient generation of inflow conditions for large eddy simulation of street-scale flows," *Flow, turbulence and combustion*, vol. 81, pp. 449–470, 2008.

[21] S. Huang, Q. Li, and J. Wu, "A general inflow turbulence generator for large eddy simulation," *J Wind Eng Ind Aerodyn*, vol. 98, pp. 600–617, 2010.

[22] N. Kornev and E. Hassel, "Method of random spots for generation of synthetic inhomogeneous turbulent fields with prescribed autocorrelation functions," *Communications in Numerical Methods in Engineering*, vol. 23, p. 3543, 2007.

[23] H. Kröger and N. Kornev, "Generation of divergence free synthetic inflow turbulence with arbitrary anisotropy," *Computers and Fluids*, vol. 165, pp. 78–88, 2018.

[24] L. Patruno and M. Ricci, "A systematic approach to the generation of synthetic turbulence using spectral methods," *Computer Methods in Applied Mechanics and Engineering*, vol. 340, pp. 881–904, 2018.

[25] R. Yu and B. Xue-Song, "A fully divergence-free method for generation of inhomogeneous and anisotropic turbulence with large spatial variation," *Journal of Computational Physics*, vol. 256, pp. 234–253, 2014.

[26] Y. Kim, I. Castro, and Z. Xie, "Divergence-free turbulence inflow conditions for large-eddy simulations with incompressible flow solvers," *Comp Flu*, vol. 84, pp. 56–68, 2013.

[27] Y. Kim and Z. Xie, "Modelling the effect of freestream turbulence on dynamic stall of wind turbine blades," *Computers and Fluids*, vol. 2016, pp. 53–66, 2016.

[28] M. Ricci, L. Patruno, and S. de Miranda, "Wind loads and structural response: Benchmarking LES on a low-rise building," *Engineering Structures*, vol. 144, pp. 26–42, 2017.

[29] L. Patruno and M. Ricci, "On the generation of synthetic divergence-free homogeneous anisotropic turbulence," *Comput. Methods Appl. Mech. Engrg.*, vol. 315, pp. 396–417, 2017.

[30] R. Kraichnan, "Diffusion by a random velocity field," *Physics of Fluids*, vol. 13, pp. 22–31, 1970.

[31] R. Vasaturo, I. Kalkman, B. Blocken, and P. van Wesemael, "Large eddy simulation of the neutral atmospheric boundary layer: performance evaluation of three inflow methods for terrains with different roughness," *Journal of Wind Engineering & Industrial Aerodynamics*, vol. 173, pp. 241–261, 2018.

[32] G. Lamberti, C. Garca-Sanchez, G. Sousa, and C. Gorle, "Optimizing turbulent inflow conditions for large-eddy simulations of the atmospheric boundary layer," *Journal of Wind Engineering and Industrial Aerodynamics*, vol. 177, pp. 32–44, 2018.